EB2020-MDS-020

Analysis of the Process Conditions for the Coating of Grey Cast Iron Brake Discs through Laser Material Deposition

Jonathan Schaible[1], Matthias Brucki[1] (*), Dr. rer. nat. Norbert Pirch[1], Thomas Schopphoven[1], Luis Andrea Hau[1], Univ.-Prof. Dr.-Ing. Dipl.Wirt.-Ing. Johannes Henrich Schleifenbaum[1,2]

[1]Fraunhofer-Institute for Laser Technology ILT
Steinbachstr. 15, 52074 Aachen, Germany (E-mail: jonathan.schaible@ilt.fraunhofer.de)

[2]RWTH Aachen University – Digital Additive Production DAP
Steinbachstr. 15, 52074 Aachen, Germany

https://doi.org/10.4672/EB2020-MDS-020

ABSTRACT: EHLA (Extreme High-speed Laser Material Deposition) is a process variant of LMD (Laser Material Deposition) that has been developed by Fraunhofer ILT and RWTH Aachen University. EHLA is characterized by the fact that the laser beam melts the powder particles above the melt pool, as opposed to conventional LMD where the particles melt only when they immerse into the melt pool. Due to this difference, EHLA processes can be set up with speeds of up to several hundred meters per minute. The changed process setup is achieved using specially designed coaxial powder nozzles and adapted process parameters. As previous work conducted at ILT has shown, EHLA allows to generate thin and uniform coatings on grey cast iron brake discs, which is desirable for different reasons, ranging from increased resistance to wear and corrosion to optical benefits and reduction of particulate emissions of vehicles. EHLA coatings as thin as 100 µm can be applied with high deposition rates (in this work up to 300 cm²/min). Compared to coatings produced by galvanic or thermal spray processes, EHLA layers exhibit a stronger metallurgical bonding to the grey cast iron substrate. In this work, a stainless steel powder material (316 L) is chosen to demonstrate the feasibility of coating grey cast iron brake discs. Process parameters based on previous experimental results are presented and compared for conventional LMD and EHLA. To underline the differences in process setup, a simulation of the two processes is performed and correlated with the experimental findings. The degree of transmission is calculated and compared as well as the temperature distribution in the substrate, focusing on the depth of the heat affected zone.

KEY WORDS: Laser Material Deposition, EHLA, Coating, Brake Disc, Wear, Corrosion

1. Introduction

1.1. Motivation for coating of brake discs

By coating brake discs with functional layers, an improvement of several properties can be achieved: (a) Increased corrosion resistance, providing benefits regarding the optical appearance as well as lifetime. This is particularly relevant in the context of e-mobility, where the majority of braking can be done using recuperation, thus increasing the time intervals between usage of the friction brakes. Corrosion can lead to optical deficiencies or to premature failure caused by surface damages of the brake discs' friction surfaces. (b) In combination with an increased wear resistance, coated brake discs can be dimensioned for automobile lifetime span and might help to provide better braking performance, e.g. reduced fading. (c) The particulate emissions caused by friction brakes are reduced. [1]

According to a study by the German Federal Environmental Agency, the wear of uncoated grey cast iron brake discs in road traffic contributes significantly to the particle emissions of a vehicle and thus to a significant environmental impact [2–4]. In addition, abrasion leading to a black pollution layer on the rims might be reduced with appropriate coatings. (d) After post-machining (grinding) of the coated brake discs, a mirror-like appearance can be achieved, marking a visual advantage, e.g. for luxury vehicles [5]. The mirror-like appearance, however, heavily depends on the grinding process and tools applied. It is impossible to achieve if pores, leading to remaining craters after the finishing, are prevalent.

Various different coating technologies for brake discs are currently under investigation. With conventional deposition welding technologies, i.e. plasma or arc deposition welding, it proves difficult to produce thin wear and corrosion protection layers in sufficient quality. Due to the comparatively large heat input, the carbon of the grey cast iron is partially dissolved in the surrounding iron matrix and the additive material, forming brittle phases, pores, bonding defects and cracks [1, 6].

1.2. LMD and EHLA for coating of brake discs

In Laser Material Deposition (LMD), a laser is used as a heat source that allows a temporarily and spatially resolved heat input into a substrate, usually metal. On the substrate surface, a melt pool is formed, into which powder particles are fed through a nozzle. The particles melt in the melt pool and contribute to a buildup of volume as the laser is moved relative to the substrate and the added material gets solidified. [7]

Extreme High-speed Laser Material Deposition (EHLA) is a novel process variant of LMD developed by Fraunhofer ILT and RWTH Aachen University. EHLA allows for high surface speeds by a

change in the process setup. As opposed to conventional LMD, the powder particles are molten by the laser above the melt pool, i.e. before they contact the substrate surface. In EHLA, the powder focus is positioned slightly above the melt pool, as illustrated in Figure 1. A continuous coaxial powder nozzle with a smaller powder focus has been designed specially for EHLA processes. [8]

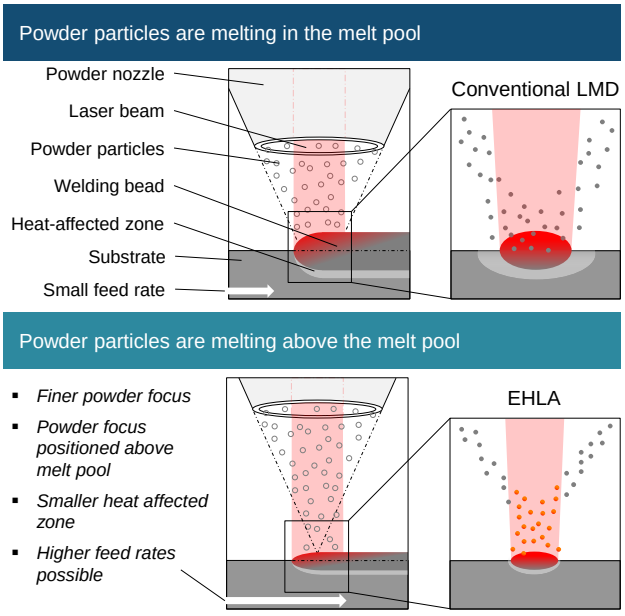

Figure 1: Schematic comparison of the interaction between laser and powder in conventional LMD and EHLA [8]

Melting of the particles above the melt pool in combination with the high surface speeds lead to the substrate temperature required for material buildup being lower compared to LMD. A smaller melt pool results in a smaller heat affected zone and a smaller dilution zone. This enables the combination of materials with different melting temperatures, e.g. titanium and aluminum, as well as the deposition of very thin, homogenous, pore-free and crack free layers with a minimal effect on the substrate. [9]

According to the patent describing EHLA [10], the process is characterized by a relative speed of at least 20 m/min, a transmission rate onto the substrate below 60 %, and a distance above the melt pool of at least 0.2 mm in which the powder material is molten.

The description of the relevant process conditions for the deposition of defect-free coatings is one major concern when pursuing qualification of LMD and EHLA as coating technology for passenger car brake discs. If the process layout and the process parameters are not tuned properly, pores can systematically form either at the interface separating two adjacent clad layers at the bonding zone or within the bulk of the layer, which is known to be detrimental to the mechanical properties.

The objective in this work is to deposit a layer that meets the criteria for both a conventional LMD process parameter set and for EHLA. Various characteristics of the two processes will be discussed with respect to this example, using the simulation results to add to this discussion.

1.3. Layer systems for coated brake discs

Grey cast iron is the most commonly used material in automotive brake discs [11]. For coating with EHLA, different layer systems can be used. The following variants have been examined at Fraunhofer ILT: (a) In addition to the stainless steel coating examined in this study, a second layer consisting of the same powder material with embedded hard particles, e.g. carbides, can be deposited on top of the intermediate layer, creating a metal matrix composite (MMC) friction layer. The bonding zone between intermediate layer and friction layer is expected to be less prone to the formation of pores and cracks compared to the graphene lamella of the grey cast iron.

The intermediate layer serves as a barrier for axial cracks that stem from the friction layer, preventing corrosive media from reaching the grey cast iron. This effect has been shown in comprehensive corrosion tests by Gramstat et al. [12].

Figure 2 shows an example of a cross section with intermediate and MMC layer. In the micrograph, two vertical cracks in the MMC layer can be seen, which are stopped at the intermediate layer, preventing corrosive media from reaching the grey cast iron.

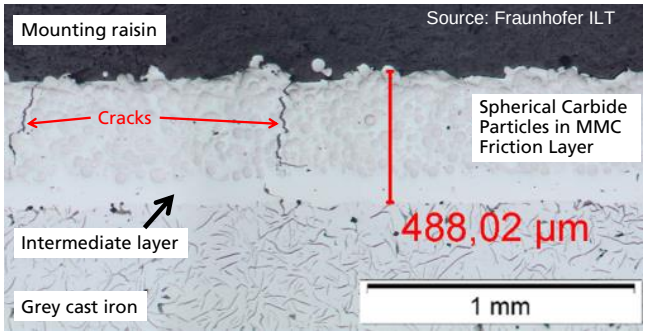

Figure 2: Cross-section of EHLA coated brake disc with intermediate layer and MMC friction layer

An additional function of an intermediate layer is the forming of a transition between the ductile grey cast iron with intrinsic damping properties and the extremely hard and brittle friction layer, relieving tension between the two materials.

(b) For applications in which extraordinary brake performance is not a necessity, e.g. for more cost sensitive electric vehicles, a single stainless steel layer may be sufficient. This is assuming that the majoritiy of braking is done via recuperation and the main function of the coating shifts towards corrosion protection.

(c) Other coating materials with favorable properties may provide similar benefits as the MMC matrix without the necessity of combining two powder types while allowing to coat the brake disc with just one layer, thus reducing complexity and, depending on the required layer thickness, process time.

2. Methods

2.1. Examined material combination

In this work, the substrate (brake disc) material is EN-GJL-180. The powder material used is stainless steel 316 L (1.4404), in

particular 316 L-A produced by Oerlikon Metco. The powder particles have a spherical shape and a size distribution in the range of 15 – 45 µm [13].

2.2. Experimental setup

The experimental setup is shown in Figure 3. The brake discs are coated on a 4-axis machine by Hornet Laser Cladding equipped with a laser processing optics head (Trumpf BEO D70) connected to a Trumpf TruDisc 4002 Yb:YAG disc laser with a maximum output of 4 kW. The powder nozzle is aligned coaxially with the laser beam axis.

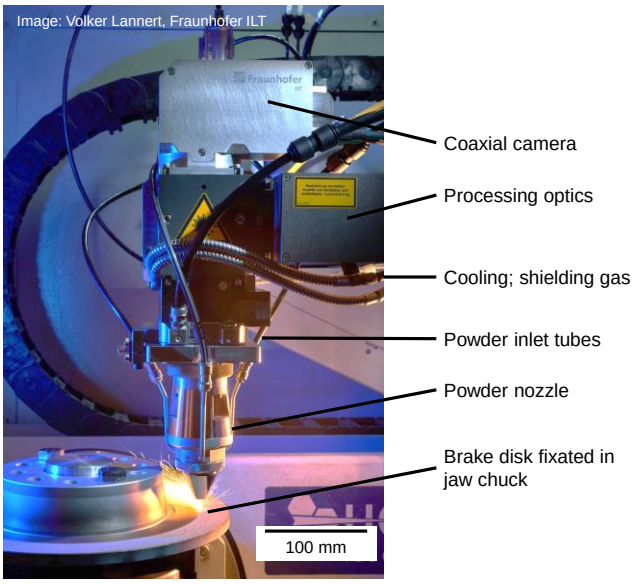

Figure 3: Experimental setup

A powder nozzle of the type ILT-Aachen-EHLA Coax D40 is positioned at a distance of 10 mm above the substrate surface for EHLA, 9 mm above the substrate for LMD. The geometrically expected distance between the nozzle tip and the powder focus is 9 mm, resulting from the angle of the conical inner and outer nozzle tips directing the powder into a conically shaped powder gas jet. Hence, in the LMD process, the powder focus coincides with the melt pool.

In the EHLA process, the powder focus is raised by 1 mm. The laser beam is focused by the processing optics with 200 mm focal length. The focal position of the laser beam is positioned on the surface of the specimen for the EHLA working distance. Argon is used as carrier gas and shielding gas. The process setups are based on experiences and previous works at Fraunhofer ILT [9, 14, 15].

2.3. Experimental methods

Several tracks of about 5 mm width were deposited onto the friction ring of grey cast iron brake discs with gaps of about 3 mm between individual tracks. In evaluating the process parameter set, criteria were the visual appearance of the process. Positive evaluation criteria are: (a) not too bright, stationary appearance of the powder gas jet during the process, (b) small amount of particles reflected back to the nozzle tip and/or adhering to the nozzle, (c) if adhesive particles are formed at the nozzle tip, good removability by a soft brush, (d) visual and haptical appearance of the deposited layers, i.e. smoothness and homogeneity of the surface and absence of visible pores, metallic color without soot or other oxidation marks.

After completion of one side of a brake disc, pieces of the brake discs were cut radially in order to obtain micrograph images perpendicular to the deposition direction. Light microscopes with magnifications fit to the examined structures were used. Positive evaluation criteria in the micrograph images are: (a) layer thickness in the expected range (i.e. calculated volumetrically from the powder mass flow rate, surface speed and lateral track offset), (b) smooth layer surface, (c) absence of pores and cracks, especially in the bonding zone between coating and grey cast iron, (d) small dilution zone and a thin and uniform appearance in the micrograph.

2.4. Modeling approach

In addition to the experimental findings, the transmission of laser radiation and substrate heating for LMD and EHLA are modelled in order to compare the experimental results. The modeling approach is based on the work of Pirch et al. [16] and Schopphoven [17].

The powder gas jet and the laser radiation are characterized experimentally and described by a mathematical model. The model's assumptions are derived from experimental observations. This allows to describe the physical process as a function of the settings for powder feed (grain fraction, powder mass flow, etc.), working distance, laser power, and feed rate.

The laser intensity distribution data from a Primes Focus Monitor measurement are approximated per plane with a super Gauss fit

$$I(x,y,z) = I_0(z)\ exp\left(-\left(\frac{r}{r_0(z)}\right)^{n(z)}\right)$$

with $r = \sqrt{x^2 + y^2}$

Standardization: $\iint I(x,y,z)dxdy = 1$.

The input measurement data for the density distributions of the powder gas jet and the fitted parameters of the super Gauss are visualized in Figure 4.

According to experimental observations with high-speed camera images of the powder gas jet, the particles are assumed to move along linear trajectories after exiting the nozzle [17]. This allows for an explicit calculation of trajectories and velocities for a statistical ensemble of particles. In order to model the particle density and thus the particle trajectories, a measuring system developed at Fraunhofer ILT was used for powder gas jet analysis. In this so-called Powder Jet Monitor (PJM), a line-shaped, horizontally aligned lateral laser illuminates the powder gas jet so that the light scattered by the particles can be captured by a coaxial camera through the center of the powder nozzle. By adding a large number of individual images (in this study: 2000), a representation of the powder density distribution in the regarded plane can be obtained. [18]

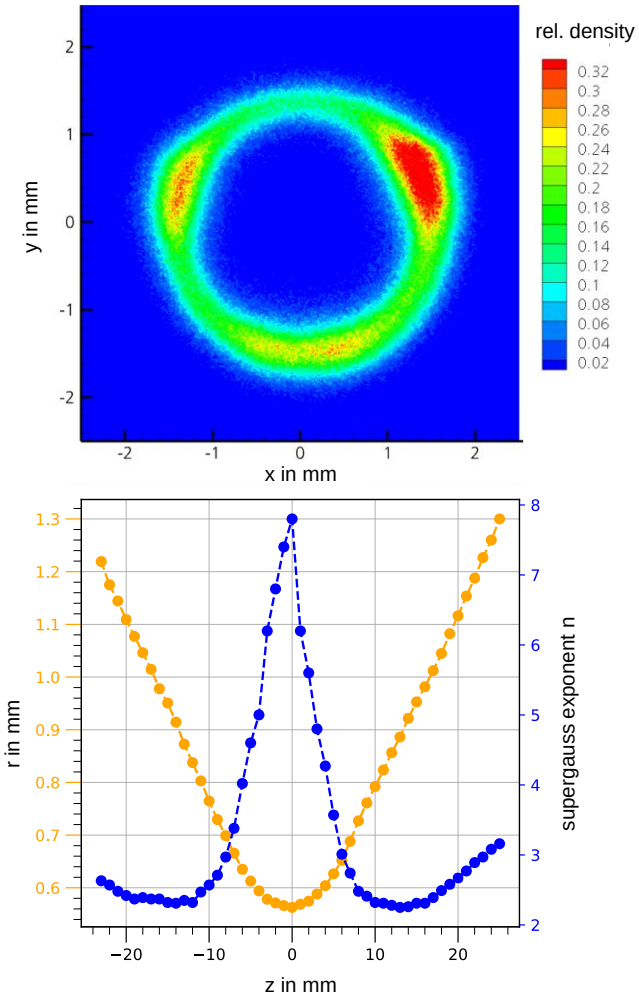

Figure 4: Relative density of the powder particle distribution in the powder gas jet 5 mm below the nozzle tip (above) and the fitted super Gauss parameters of the laser beam in different planes z (below)

In contrast to the approach of Schopphoven [17] where the particle velocity is determined indirectly by counting the particles within a defined control volume, the particle velocity is determined directly from high-speed video recordings of the powder gas jet in absence a laser beam. By means of the spatial and temporal difference between successive frames, an average powder particle velocity can be calculated.

With known initial laser intensity distribution along the beam axis, the degree of transmission of laser radiation onto the substrate surface can be calculated in a space-resolved manner as a function of powder mass flow, powder size distribution and particle velocity. This allows to calculate the particle temperature and the temperature distribution of the substrate.

Figure 5 shows a schematic picture of the combined mentioned simulation tools for an LMD process.

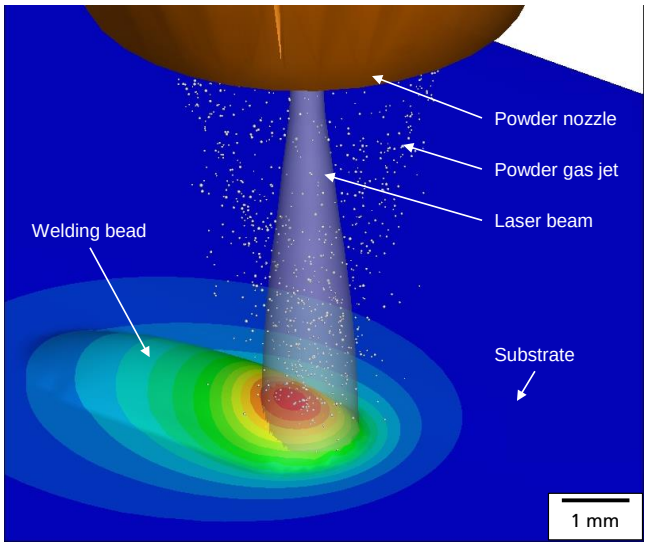

Figure 5: Schematic view of the simulation components

3. Results

3.1. Experimental Results

The final process parameter sets presented in the following were found using an iterative approach based on the evaluation criteria listed in Section 2.3.

The motorized collimation is left at a constant 0 mm focus shift for both processes. Hence, the interaction between laser beam and powder gas jet is kept the same above the powder focus. However, with the distance between substrate and powder nozzle differing by 1 mm and different carrier gas flow rates determining particle velocity, the interaction distance and time are different for the two regarded processes. For the EHLA process, the stand-off between nozzle tip and substrate is set to 10 mm, i.e. focus of the powder gas jet lies 1 mm above the melt pool, and the laser focus is positioned on the surface level with a resulting laser spot diameter of 1.178 mm. For the LMD process, the stand-off is reduced to 9 mm so that the powder focus is on the level of the melt pool. The laser spot diameter on that level is slightly bigger at about 1.182 mm.

For conventional LMD, a process speed of 2.5 m/min was chosen in order to reach the range considererd as typical [7], with 2.5 m/min marking the lowest achievable speed with the system technology used.

There seems to be a threshold at about 900 W laser power, above which, with the used system technology, the graphene lamella cause a strongly flickering process and induce large macroscopic crater-like pores. Above this threshold, particles and/or melt pool mass recoiled back at the powder nozzle. This effect could be observed indirectly via the increased occurrence of adhering particles at the nozzle tip, which causes a degradation of the powder gas jet symmetry.

In order to avoid those problems, the laser power and the powder mass flow rate were reduced accordingly in an iterative approach. The results were rated based on the visual behavior of the process

(calm vs. flickering, apparent brightness of the interaction zone with glowing particles), the visual and haptical appearance of the layers, and the obtained micrographs of the cross-sections from the coated brake discs. Evaluation criteria are low porosity, homogenous appearance and absence of cracks in the deposited layer. The bonding zone between the deposited layer and the substrate material is of particular interest; criteria for good metallurgical bonding are: thin, uniform bonding zone with low porosity, free of cracks, small heat affected zone, no creation of brittle intermetallic phases.

The process parameters listed in Table 1 were chosen as the final parameters.

Table 1: Final process parameters

Parameter	EHLA	Conventional LMD
Focus shift of motoric collimation	0 mm	0 mm
Laser spot diameter on substrate	1.178 mm	1.182 mm
Stand-off nozzle/substrate	10 mm	9 mm
Laser power	2800 W	850 W
Lateral track offset	0.15 mm	0.6 mm
Surface speed	200 m/min	2.5 m/min
Powder mass flow rate	33.0 g/min	8.0 g/min
Carrier gas flow rate (Ar)	9 l/min	5 l/min
Shielding gas flow rate (Ar)	10 l/min	5 l/min

Figure 6 provides a visual impression of the brake disc coated with the final process parameters. Both layers have a homogenous macroscopic appearance without irregularities such as pores. The corresponding micrographs are shown in Figure 7. The LMD layer in the upper micrograph has a very smooth surface and the bonding zone meets the criteria presented above. However it is clearly visible that the dilution zone is larger and that the added powder material partially intrudes into the grey cast iron, going down below the initial surface level.

In contrast, the bonding zone of the EHLA layer in the lower image is extremely small and a uniform metallurgical connection is apparent. Porosity in the bonding zone is slightly more prevalent with the regarded EHLA parameter set. The surface is rougher compared to LMD. Individual particles that might not have been entirely melted can be spotted sticking out from the surface. The LMD layer displays (most likely heat-induced) cracks in the bonding zone. Those cracks bear the risk to further propagate with an added friction layer.

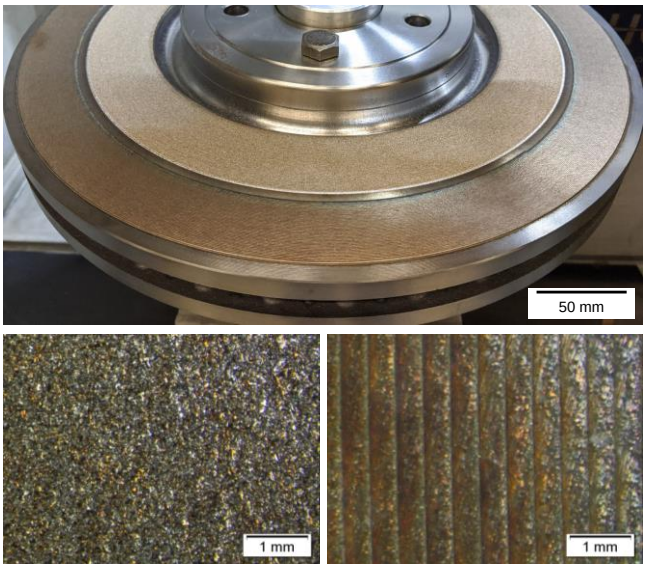

Figure 6: Photograph of the partially coated brake disc (above; EHLA layer on the inside) and macro images of the surfaces (below; EHLA on the left)

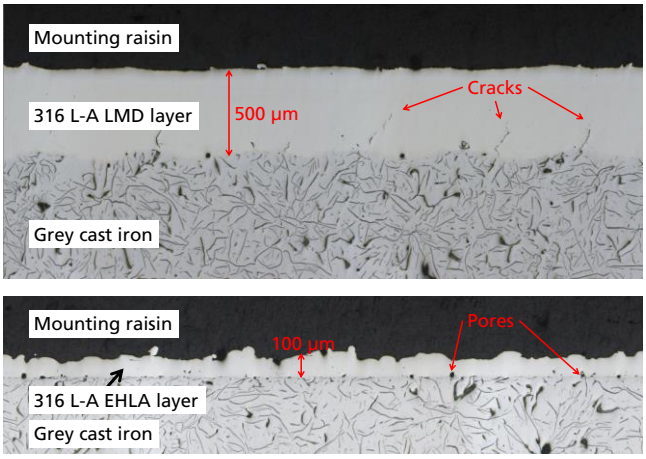

Figure 7: Micrograph images of both final parameter layers: LMD layer (above) and EHLA layer

Further measurement results are presented in Table 2. With EHLA, the process time is smaller by a factor of 20 compared to conventional LMD. However, this is not taking into account the different layer thicknesses. The target layer thickness depends on the requirement for the lifetime, the friction pairing, and the appearance of the coated brake disc. In the two particular process points compared in this work, the powder efficiency of the EHLA process is better at 83.6 % vs. 70.9 % in LMD. A possible reason lies in the fact that the particles are heated before touching the substrate, enabling some particles that land outside of the laser spot to stick to the surface as well. In LMD, particles that land outside of the melt pool are mostly lost with respect to track formation.

Table 2: Measurement results

Parameter	EHLA	Conventional LMD
Powder efficiency	83.6 %	70.9 %
Mean powder particle velocity for respective parameter setup (without laser)	8.80 m/s	5.67 m/s
Surface deposition rate	300 cm²/min	15 cm²/min
Layer thickness above substrate level (from micrograph)	80–100 µm	500 µm
Hardness (average of 6 measured values)	217 HV 0.3	216 HV 0.3

3.2. Model-theoretical results

To illustrate the essential process differences between LMD and EHLA, the heat distribution in the substrate material and the transmission of the laser radiation between the two process variants is compared on the basis of the model by Pirch et al. [16]. In analogy to Schopphoven [17], the spatially resolved transmission distribution can be calculated on the basis of the measured powder gas jet. Figure 8 shows the transmission distribution for the two used experimental setups.

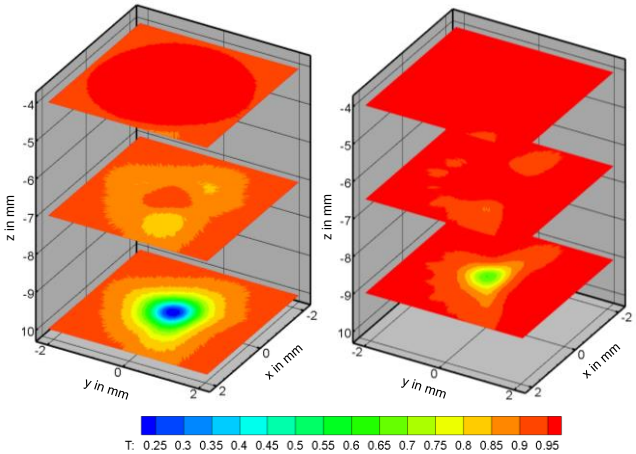

Figure 8: Simulated spatial distribution of transmission T for the EHLA setup (left) and for the LMD setup

It can be seen that the transmittance in the working plane of the EHLA setup at z = –10 mm drops to 20 %, whereas the transmittance in the working plane of the LMD setup at z = –9 mm just drops to 60 %. The main reasons for this difference are the shorter shading distance (1 mm less) in the LMD setup and the lower powder mass flow of 8 g/min in comparison to 33 g/min. The characteristic asymmetries in the plane related transmittance distribution shown in Figure 8 is due to the characteristics of the powder gas jet (cf. measured particle density distribution in Figure 4), in which three local maxima are formed between adjacent powder supply inlets of the coaxial powder nozzle.

With the calculated transmission distributions it is possible to calculate the total proportion of transmitted energy on the substrate surface. Figure 9 shows the proportion of transmitted energy as a function of the powder mass flow for both setups.

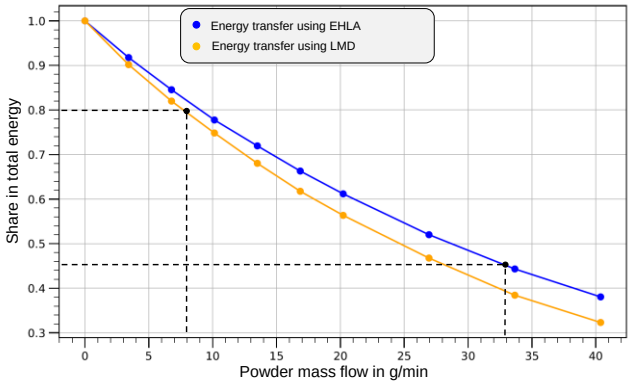

Figure 9: Simulated share of transmitted energy in total energy depending on the powder mass flow

The black dots marked in Figure 9 represent the two process points used. For the LMD parameter set, the transmitted part of the energy is about 80 % and for the EHLA parameter set about 45 %.

It can be seen that, for an identical powder mass flow, the transmitted energy is higher for the EHLA setup than for the LMD setup, although the range of shading by the powder gas jet is 1 mm larger. This results from the greater carrier gas flow rate in the EHLA setup (9 l/min instead of 5 l/min) causing the significantly higher average powder particle velocity (Table 2), which in turn reduces the number of powder particles per volume and increases the transmission. Through this interrelation, the carrier gas volume flow rate plays a decisive role in the energy distribution between substrate and powder material.

For the used process points the transmission reduction for the EHLA setup means that, in contrast to the LMD setup, the majority of the irradiated energy is fed into the powder gas jet. Thus, the powder particles are molten above the substrate surface, which allows to significantly increase the feed rate. Both the local existence time and the depth of the melt pool can be much smaller than in LMD, where the powder particles have to be molten in the melt pool on the substrate surface [17].

The less pronounced melt pool implies a reduced heat input into the substrate material in EHLA processes. In order to avoid the influence of the heated powder particles, the heat distribution with unshaded intensity is considered in the simulation results below. This allows a statement to be made about the maximum melt pool expansion. Figure 10 shows the quasi-stationary substrate temperature distribution of the two parameter sets in the single track cross section.

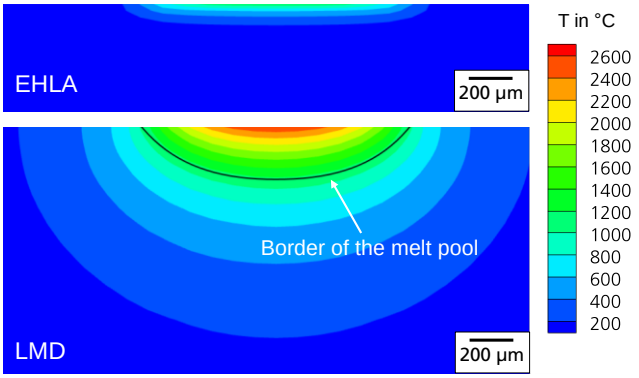

Figure 10: Simulated quasi-stationary substrate temperature distribution in the single track cross section for a laser power of P = 2800 W and a feed rate of v = 200 m/min (top) or P = 850 W and v = 2.5 m/min (bottom) without shading effect of powder gas jet

The solid black line in Figure 10 confines the area above the grey cast iron melting temperature of approx. 1135 °C [19]. The necessary temperature-dependent material values were taken from Mills material parameters [19]. In addition, the absorption of grey cast iron was set to 32 % [20]. The resulting melting bath depth is approx. 240 µm for the LMD parameter set and approx. 3.5 µm for the EHLA parameter set.

This simulative result can be correlated with the appearance of the bonding zone in the micrographs shown in Figure 7: In LMD, the coating goes down below the initial surface level with each weld bead, whereas in EHLA, the bonding zone is very thin and exactly on the initial surface level throughout the entire image.

4. Conclusion and Outlook

In this work, several aspects of conventional LMD and EHLA have been compared with respect to coating of grey cast iron brake discs with a 316 L layer. In an experimental comparison, two parameter sets that allow coating with thin layers of low porosity, therefore promising good corrosion resistance, have been presented. Closed EHLA layers as thin as 100 µm can be deposited with a thin and uniform metallurgical bonding. The presented LMD parameter set yields a layer thickness of about 500 µm at a significantly lower surface coating rate.

Nevertheless, with further parameter adaption it should be possible to lower the tendency for crack formation in the LMD layer, while at the same time getting thinner layers with higher surface coating rates, e.g. by using a larger laser spot diameter. However, since two orders of magnitude separate the surface speeds used in this work, EHLA productivity is expected to remain unmatched by LMD with the regarded material combination and system technology. In conclusion, LMD and especially EHLA, offer a promising way for applying wear and corrosion resistant coatings to brake discs.

The model theoretical investigations carried out show the differences of the transmittance and of the maximal heat-affected zone between the used LMD and EHLA setups. In the LMD setup presented in this study, the transmitted power is about 80 %, whereas in the EHLA setup, it is about 45 %. Due to the lower transmitted energy and higher feed rates in EHLA, the heat-affected zone in the substrate material is much smaller. This finding is in accordance to the experimental results.

Further additions to the simulation model could include the effect of particles that are accelerated by repulsion caused by partial evaporation [21, 22]. This effect is expected to have a significant influence on the particle velocity distribution, thus also on the shading and on the energy distribution between powder and substrate. Including the effect of accelerated particles would allow to make more accurate predictions of laser-particle interaction and therefore powder efficiency.

The MMC friction layer and the effects that carbides with higher melting temperatures (compared to the matrix materials) have on the layer formation could also be examined in the simulative approach. With those additions to the simulation, the theoretical results could help to reduce the number of experiments required in the process development.

References

[1] Markus Harke, “Verfahren zum Erzeugen einer verschleiß- und/oder korrosionsfesten Beschichtung auf einer Reibfläche eines Bremskörpers sowie nach dem Verfahren herstellbarer Bremskörper,” DE 10 2016 200 951 A1, Germany.

[2] Dan Wakeling, Tim Murrells, David Carslaw, John Norris, and Luke Jones, The Contribution of Brake Wear Emissions to Particulate Matter in Ambient Air: Final Report. [Online]. Available: https://www.vda.de/dam/vda/publications/2017/FAT/FAT-Schriftenreihe_301.pdf (accessed: May 6 2020).

[3] World Health Organization, Regional Office for Europe, “Review of evidence on health aspects of air pollution - REVIHAAP Project,” 2013. Accessed: May 6 2020. [Online]. Available: http://www.euro.who.int/__data/assets/pdf_file/0004/193108/REVIHAAP-Final-technical-report.pdf

[4] Umweltbundesamt, Ed., “Feinstaubbelastung in Deutschland,” Accessed: May 6 2020. [Online]. Available: https://www.umweltbundesamt.de/sites/default/files/medien/publikation/long/3565.pdf

[5] Thorsten Elbrigmann, Hart wie Diamant. [Online]. Available: https://christophorus.porsche.com/de/2017/384/porsche-surface-coated-brake-cayenne-turbo-development-center-weissach-diamond-14479.html (accessed: Jan. 25 2020).

[6] J. Nurminen, J. Näkki, and P. Vuoristo, “Laser cladding on cast iron substrates,” in International Congress on Applications of Lasers & Electro-Optics, Miami, Florida, USA, Oct. 2005, P534.

[7] A. Gebhardt, Additive Fertigungsverfahren: Additive Manufacturing und 3D-Drucken für Prototyping - Tooling - Produktion, 5th ed. München: Hanser, 2016.

[8] T. Schopphoven, A. Gasser, and G. Backes, “EHLA: Extreme High-Speed Laser Material Deposition,” LTJ, vol. 14, no. 4, pp. 26–29, 2017, doi: 10.1002/latj.201700020.

[9] T. Schopphoven, A. Gasser, K. Wissenbach, and R. Poprawe, “Investigations on ultra-high-speed laser material deposition as alternative for hard chrome plating and thermal spraying,” Journal of Laser Applications, vol. 28, no. 2, p. 22501, 2016, doi: 10.2351/1.4943910.
[10] W. Küppers, G. Backes, and J. Kittel, “Extremes Hochgeschwindigkeits-Laserauftragschweißverfahren,” DE 10 2011 100 456 A1.
[11] B. Breuer, Ed., New material technologies for brakes: XIX International [my]-Symposium, Brake Conference, 29/30 October 1999, Bad Neuenahr/Germany. Düsseldorf: VDI-Verl., 2000.
[12] Sebastian Gramstat, “Hard-metal Coated Brake Discs - Investigations of Tribology, Mechanical Robustness and Wear Products: Eurobrake 2019, EB2019-MDS-020,”
[13] OC Oerlikon Corporation AG, Material Product Data Sheet: DSMW-0017.2 – Austenitic Steel for Laser Cladding. [Online]. Available: https://www.oerlikon.com/ecomaXL/files/metco/oerlikon_DSMW-0017.2_AusteniticSteel_LC.pdf&download=1 (accessed: May 6 2020).
[14] T. Li et al., “Extreme High-Speed Laser Material Deposition (EHLA) of AISI 4340 Steel,” Coatings, vol. 9, no. 12, p. 778, 2019, doi: 10.3390/coatings9120778.
[15] Ingomar Kelbassa, “Qualifizieren des Laserstrahl-Auftragschweißens von BLISKs aus Nickel- und Titanbasislegierungen,” Fakultät für Maschinenwesen, Rheinisch-Westfälischen Technischen Hochschule, Aachen, 2006.
[16] N. Pirch, S. Linnenbrink, A. Gasser, K. Wissenbach, and R. Poprawe, “Analysis of track formation during laser metal deposition,” Journal of Laser Applications, vol. 29, no. 2, p. 22506, 2017, doi: 10.2351/1.4983231.
[17] Thomas Schopphoven, Experimentelle und modelltheoretische Untersuchungen zum Extremen Hochgeschwindigkeits-Laserauftragschweißen. Ph.D. Thesis. Aachen, Germany, 2020.
[18] S. Mann, L. de Melo, and P. Abels, “Measurement of particle density distribution of powder nozzles for laser material deposition,” in International Congress on Applications of Lasers & Electro-Optics, Miami, Florida, USA, Oct. 2013, pp. 370–375.
[19] K. C. Mills, Recommended Values of Thermophysical Properties for Selected Commercial Alloys. Cambridge: Woodhead, 2002.
[20] E.M.R. Silva, W.A. Monteiro, W. Rossi, M.S.F. Lima, “Absorption of Nd:YAG laser beam by metallic alloys,” JournaI of Materials Science Letters 19, pp. 2095–2097, 2000.
[21] I. O. Kovaleva and O. B. Kovalev, “Effect of the recoil pressure induced by evaporation on motion of powder particles in the light field during laser cladding,” J Appl Mech Tech Phy, vol. 53, no. 1, pp. 56–66, 2012, doi: 10.1134/S0021894412010087.
[22] T. Mitra, A. K. Brown, D. M. Bernot, S. Defrances, and J. J. Talghader, “Laser acceleration of absorbing particles,” Optics express, vol. 26, no. 6, pp. 6639–6652, 2018, doi: 10.1364/OE.26.006639.